Applied Surface Science 389 (2016) 260–269

Contents lists available at ScienceDirect

Applied Surface Science

journal homepage: www.elsevier.com/locate/apsusc

Effect of individual discharge cascades on the microstructure of plasma electrolytic oxidation coatings

S.C. Troughton[a], A. Nominé[b], J. Dean[a], T.W. Clyne[a,*]

[a] *Department of Materials Science & Metallurgy, Cambridge Universitym 27 Charles Babbage Road, Cambridge CB3 0FS, UK*
[b] *Department of Physical Sciences, Open University, Walton Hall, Milton Keynes MK7 6AA, UK*

ARTICLE INFO

Article history:
Received 20 May 2016
Received in revised form 12 July 2016
Accepted 16 July 2016
Available online 19 July 2016

Keywords:
Plasma electrolytic oxidation
Electrical discharge
High speed photography
X-ray tomography
Microstructure

ABSTRACT

Short duration (~1 s) PEO treatments have been applied to aluminium alloy samples on which coatings of thickness ~100 μm had previously been created. This was done using the small area electrical monitoring system previously developed in the Gordon Laboratory in Cambridge. Voltage supply frequencies of 50 Hz and 2.5 kHz were employed. Fairly high resolution SEM micrographs were taken, covering the whole surface of small area samples (ie over a circular area of diameter about 0.9 mm). This was done both before and after the 1 s PEO treatments. X-ray tomographic data were also obtained in the vicinity of a recently-completed set of discharges. The outcomes of these observations were correlated with synchronised high speed electrical monitoring and video photography, carried out during the PEO treatment periods. Localised cascades (comprising hundreds of individual discharges) were observed in all cases, persisting throughout the 1 s periods and also reappearing in the same location when a second 1 s PEO treatment was applied to the same sample. This repetition of discharges at the same location is apparently due to the deep pores associated with these sites, creating a pathway of low electrical resistance, even after appreciable oxidation has occurred in the vicinity. Observations were made of the way in which the surfaces were reconstructed locally as discharge cascades occurred. With the high frequency voltage supply, discharge lifetimes were limited to the half-cycle period (of 200 μs), but in other respects the cascades were similar to those with the lower frequency. However, some discharges occurred during cathodic half-cycles with the high frequency supply, at the same location as the anodic discharges in the cascade concerned.

1. Introduction

Progress continues to be made on improved understanding of the complex phenomena that take place during plasma electrolytic oxidation (PEO) processing, particularly relating to the temporal, spatial and electrical characteristics of individual discharges. For example, the strong tendency for them to occur in long sequences ("cascades"), in specific locations, is now clearly established [1–7], with typical discharge lifetimes (~30–300 μs), "incubation" periods between discharges (~0.1–1 ms), peak discharge currents (~10–100 mA), discharge energies (~1–10 mJ) and diameters of core discharge channels (~10–100 μm) all becoming fairly clear (although far from uniform during a given treatment and quite sensitive to processing conditions). Some correlations have been established [5,8,9] between external conditions, discharge characteristics and features of resultant coatings, including the coating growth rate, and progress has also been made [6,7,10] on correlating the energetics of individual discharges with that of the process as a whole (with the ultimate aim of reducing the – often relatively high – rate of energy consumption).

One feature that has been noted and studied [2,4,6,11,12] is that gas bubbles (or "plasma bubbles") form in the region where an individual discharge emerges into the electrolyte, with a tendency to grow rapidly into relatively large hemispheres (and then to shrink). Recent work [7] has focused on this phenomenon and highlighted the fact that much of the energy absorbed during the process goes into vaporization of water at the top of the plasma channel, leading to rapid expansion and contraction of a large gas bubble at that location, with most of the energy finally going into heating of the electrolyte. Other points of interest include recent observations [13–16] that discharges can under some circumstances occur during the cathodic part of the cycle, although clear links have not yet been established between the conditions that promote this and the mechanisms that might create such discharges.

However, while many of the phenomena that commonly occur during PEO processing have been studied in some detail, using a

---

* Corresponding author.
E-mail address: twc10@cam.ac.uk (T.W. Clyne).

http://dx.doi.org/10.1016/j.apsusc.2016.07.106

variety of electrical, optical and spectroscopic techniques, there has been very little in the way of correlating the discharges directly with the resultant coating microstructure, despite the fact that this is likely to have a profound influence over the performance of the coating in service. Of course, there have been many studies of coating growth rates and mechanisms [17–19], the level and nature of coating porosity [20–22], the creation of residual stresses [23] etc, but these have all been tackled in terms of the overall outcome of many discharge cascades distributed (temporally and spatially) in a complex way over the whole sample and over extended processing periods. The (localised) microstructural changes created by a well-defined discharge cascade have not previously been examined. The present paper is focused on this issue, encompassing the effects of supply frequency, interruption of the process and differences between the nature of anodic and cathodic discharges.

2. Experimental procedures

2.1. Sample preparation

PEO coatings were produced on Al-2014 substrates, in the form 2 × 25 × 25 mm plates mounted in resin. A small piece of the plate material was swaged to produce a wire of diameter 0.88 mm. This wire was mounted in the resin, adjacent to the plate. Wire and plate were connected to a pair of PVC-insulated twisted wires extending out of the tank, where a 50 Ω resistor and reed relay switch (Coto Technology 9104-05-11) connected the ends of the wires. Further details of the set-up are provided in previous papers [1,2,4,7].

Coatings were prepared using a 100 kW Keronite^{TM} processing rig and an electrolyte consisting primarily of a dilute aqueous solution of potassium hydroxide and sodium silicate. The electrolyte was maintained at a temperature of approximately 20 °C by re-circulation through a heat exchanger. The applied potential was nominally square-wave, with a frequency of either 50 Hz or 2500 Hz. A constant current condition was set, corresponding to a current density of 31 A dm^{-2}, for both anodic and cathodic polarities. The applied voltage was therefore not pre-determined, but adjusted by the power supply to maintain the appropriate current. Samples were processed for 30 min prior to initial SEM imaging of the sample surface, creating PEO coatings about 100 μm in thickness.

2.2. High speed video capture and analysis

The camera employed was a Phantom V12.1, with the acquisition rate set at 180,064 frames per second (5.12 μs exposure time). Images were recorded with 12-bit resolution. The linear spatial resolution was 13 μm per pixel. Typical images comprised 128 × 128 pixels, covering the whole small area sample (circle of diameter 0.88 mm). Sample surfaces were viewed through a glass window in the electrolyte tank. The distance between lens and sample was typically about 300 mm.

Video image sequences were superimposed over both the complete 1 s period (~180,000 frames) and also over single half-cycles at the 2.5 kHz frequency, ie periods of 200 μs, comprising 36 frames. In both cases, there was no external illumination, so the images were affected only by light emission (from discharges) on the surface of the sample. Bubble growth occurs from the point at which the discharge reaches the surface [7], which has the effect of reducing the sharpness of the images in the vicinity of the discharges, but their location is nevertheless clearly revealed.

2.3. Small area current monitoring

The small area electrical monitoring technique is described in detail elsewhere [1,2,4,7]. Electrical data were collected using a four-channel, 8-bit resolution PC oscilloscope (Pico Technology, Picoscope 6403), with a sample interval of 480 ns. The voltage across the electrolyte tank was measured using an active differential probe (Pico Technology TA043) with 100 × attenuation. The end of the wire was used as the small area sample. The wire was connected to a bulk substrate through a 50 Ω resistor and a reed relay switch, with the current determined from the voltage drop across the resistor, which was measured using an active differential probe (Pico Technology TA043) with 10 × attenuation. This created a current scale range of ±400 mA, which covered all of the profiles except for a few peaks during cathodic discharges.

An arbitrary function generator (TTi TG1010A Programmable 10 MHz Function Generator) was used to supply a single square wave pulse of +5 V of duration one second. This signal was used to trigger the recording of the oscilloscope and high speed camera, as well as supplying power to the reed relay switch allowing it to complete the circuit between the small area and bulk samples. This ensured the camera, oscilloscope and short treatment were all initiated at same time, giving synchronised data.

2.4. SEM Microscopy and Image Processing

After initial PEO processing for 30 min, samples were removed from the electrolyte, washed in de-ionised water and dried in a stream of warm air. Samples were then sputtered with a thin layer of gold for SEM observation. The entire small area sample (end of the 0.88 mm diameter wire) was imaged in back-scattered electron mode, in a CAMSCAN microscope, using an accelerating voltage of 10 kV and a working distance of 33 mm. A complete map of the sample surface was created by stitching ~16 images together in Photoshop. After a short (1 s) PEO treatment had been applied to the small area sample, as described in §2.1, SEM imaging was carried out again. This was done twice in sequence on the same sample with a 50 Hz supply and once (on a different sample) at 2.5 kHz.

2.5. X-ray Computed Micro-Tomography

The specimen was scanned using a Skyscan 1172 X-ray microtomograph. The resolution was ~1.2 μm. Serial sections (in the form of a stacked set of radiographs) were imported into ScanIP (software for 3D imaging, visualisation and analysis). Prior to reconstruction of the 3D geometry, the radiographs were thresholded, using in-built segmentation algorithms, and surfaces were smoothed using a recursive Gaussian filter.

3. Electrical, video optical and microstructural monitoring

3.1. Electrical characteristics for low and high frequency

Typical variations of voltage and (small area) current are shown in Fig. 1 for (a) 50 Hz and (b) 2.5 kHz. It can be seen in Fig. 1(a) that 7 discharges occurred during this anodic half-cycle (10 ms period) at 50 Hz. The anodic voltage developed was about 600 V. The average current during this cycle was about 20 mA. During the 1 s treatment period, discharges occurred only during the latter part, such that the average anodic current over the whole period was about half this value. The average current during the cathodic half-cycles tended to be more homogeneous and was also ~10 mA, although the voltage needed to create this was only ~150 V. Converted to a current density, using the nominal surface area of the wire, a current of 10 mA corresponds to about 200 A dm^{-2}, which is larger by a factor of about 6 than the pre-set value (which flows through

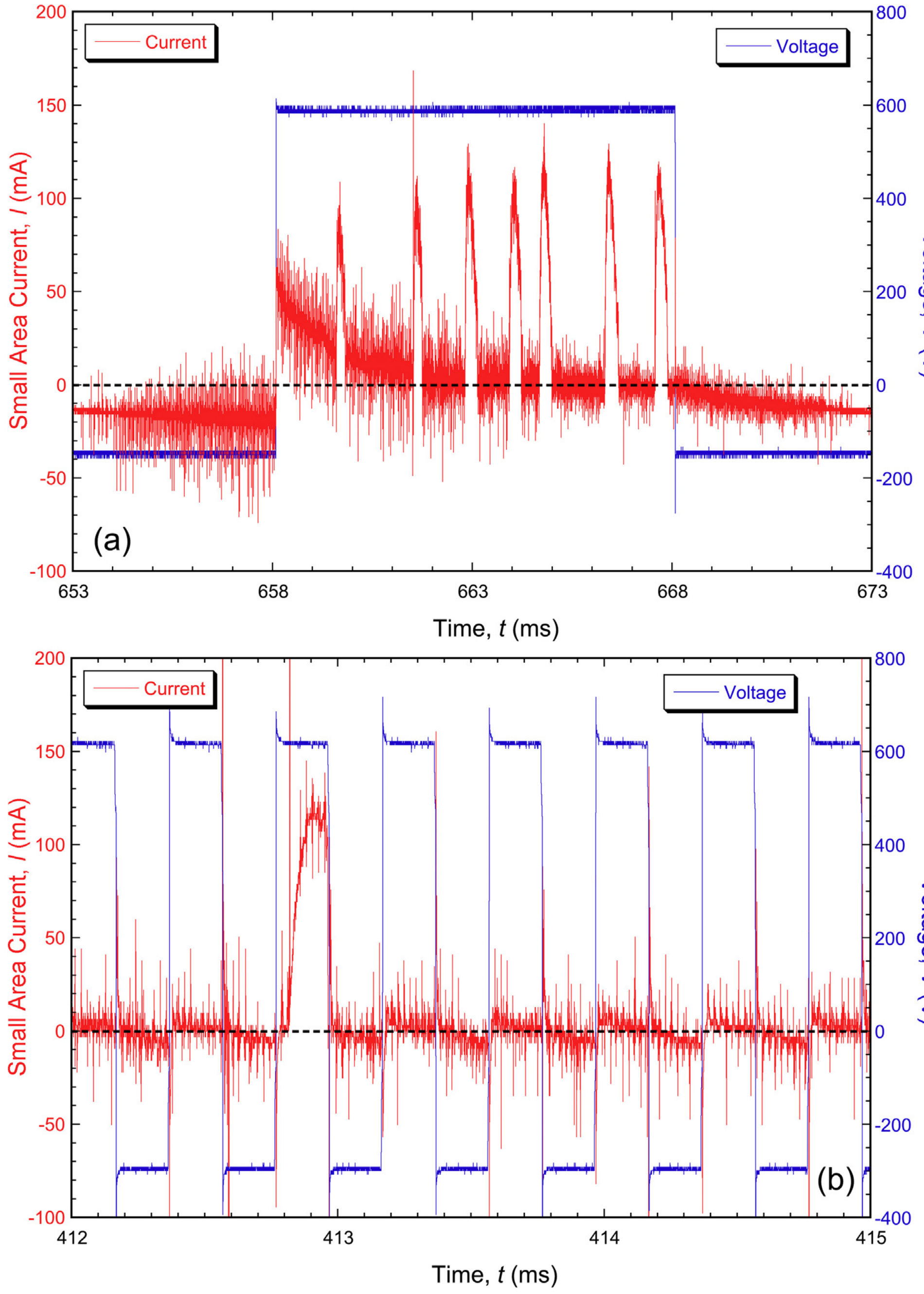

Fig. 1. Synchronised plots of (small area) current and voltage during representative periods for supply frequencies of (a) 50 Hz and (b) 2500 Hz.

the main part of the sample). This difference is partly attributed to the convergent nature of the electric field in the vicinity of the small area sample (analogous to the "corner effect" often observed with bulk samples) and also to some coating production on the cylindrical surface of the wire exposed by the small interfacial gap between it and the surrounding resin. (It should also be noted that the period of 1 s is rather short for the discharge characteristics on the small area sample to be expected to conform to overall average behaviour.) Typical peak discharge currents were ~100 mA and discharge lifetimes were ~300 μs. These values are consistent with previous reports [6,7], which confirmed that prolonged sequences of discharges ("cascades") tend to occur in the same location.

With the higher frequency supply (Fig. 1(b)), the average current was similar to that at 50 Hz (~10 mA), in both anodic and cathodic half-cycles, but there was sufficient time for only a single discharge in an individual anodic half cycle and these occurred in only a relatively small proportion of them. The voltage created during the anodic half cycles was similar to that with the lower frequency (~600 V), but in the cathodic half-cycles it was larger (~300 V, compared with 150 V), suggesting that a larger driving force is required to maintain the set current density when the frequency is high. Typical periods between (anodic) discharges were about 5 ms, corresponding to about 12 cycles. The peak current in a discharge (~100 mA) was similar to the low frequency case. Discharge lifetimes commonly covered the whole half-cycle period (200 μs), suggesting that they were being cut slightly short as the voltage switched to cathodic.

It was also noticeable that, with the high frequency voltage, discharges sometimes occurred during the cathodic part of the cycle. This is illustrated in Fig. 2, where it can be seen that they commonly, but not invariably, followed an anodic half-cycle in which a discharge had occurred. It can also be seen that, while the dis-

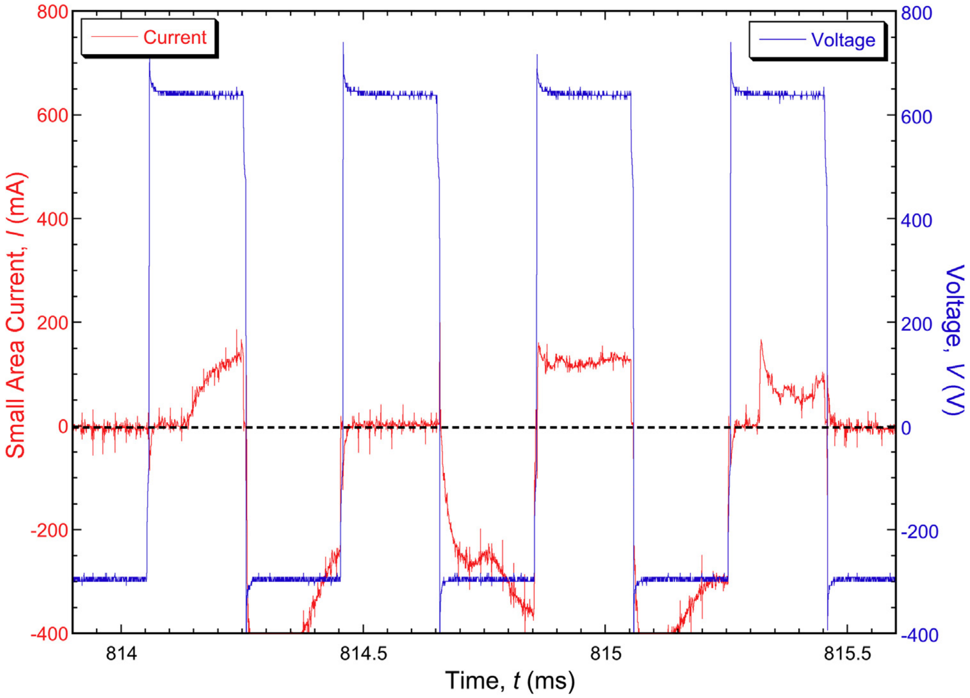

Fig. 2. Synchronised plots of (small area) current and voltage during PEO processing at 2500 Hz, showing a set of cathodic discharges.

charge lifetime was usually the half-cycle period (200 μs), the peak current (~300–400 mA) was significantly larger than that during anodic discharges (~100 mA). They do take place with a lower voltage (~300 V, as opposed to 600 V for anodic discharges), but the levels of energy, as well as the amount of charge transferred, do therefore appear to be somewhat greater for cathodic discharges – see §3.4 below. The cathodic discharges were less common than the anodic ones, but, as can be seen in Fig. 2, they tended to occur in clusters. It seems likely that oxidation takes place during cathodic discharges in a similar way to that in anodic ones, since both presumably allow exposure of metal from the substrate to oxidizing agents in the plasma channel.

It may also be noted that, under all conditions employed in the current work, discrete, well-defined discharges were observed, so that “soft” sparking, which has occasionally been reported to take place during PEO processing (without well-defined individual discharges), did not occur.

3.2. Microstructural evolution during discharge cascades

On comparing SEM micrographs before and after the short duration (~1 s) PEO treatments, it was immediately apparent that changes had occurred in one region only, despite the fact that many discharges had been generated during this period. This is strong evidence for the localization of cascades, and also suggests that they can persist in a given location for considerably extended periods (during which hundreds of discharges occur). An example can be seen in Fig. 3, which shows micrographs taken before and after a PEO treatment at 50 Hz, lasting for 1 s. Discharges occurred only during the last 0.6 s of this period (through about 30 cycles), with a total of about 250 discharges (about 8 or so in each anodic half-cycle) during this treatment. These discharges all occurred in the upper central region of the sample (as oriented in Fig. 3). Evidence for this is presented in Fig. 4, which shows a single video frame (from an anodic half-cycle) and also the complete set of superimposed frames (with ~5 μs exposure time) over the 1 s period. It can be seen that significant light emission occurred only in the two (adjacent) locations in Fig. 3(c) where the microstructure had changed. (It should be appreciated that relatively large gas bubbles normally form at the top of plasma channels in such coatings [7], blurring the sharpness of the light emission in images of this type.)

The only region in Fig. 3(a) in which the microstructure differed significantly before and after the 1 s PEO treatment was the upper central area shown at higher magnification in Figs.Fig. 3(b) and Fig. 3(c). As can be seen in these two micrographs, changes were induced by the repeated discharges in the central part of this field of view (particularly in the two regions indicated by the dotted circles). It does appear in this case that microstructural changes at the surface, and associated emission of light, were centred on two locations about 200 μm apart, and the affected regions were approximately circular, with diameters of the order of 100–150 μm. Emissions often occurred simultaneously from both locations (see Fig. 4(a)), although there were also instances in which one or the other dominated. It seems likely that they were both associated with the same discharge events, probably with the same point of origin at the interface between coating and substrate, but different paths to the surface. (Previous observations [6] have suggested that independent simultaneous discharge cascades are unlikely to be located much closer than about 1 mm apart and this is in line with broad expectations concerning the nature of associated electric fields and charge redistribution effects.) It may be that such a bifurcation of discharge paths to the surface is relatively rare, although these observations confirm that it can happen.

It has been estimated in previous publications [6,7] that a typical discharge energy is ~1 mJ under the conditions used in the present work and that the conversion rate between discharge energy and resultant volume of coating is typically ~10^{13} J m^{-3} (10^{-5} J μm^{-3}). Of course, these are highly approximate figures, but it follows that, during the 1 s PEO treatment, with ~300 localised discharges occurring on the small area sample, about 0.3 J of energy was absorbed there, creating ($0.3/10^{-5}$) ~3×10^4 μm^3 of oxide: this corresponds to a cube of side ~30 μm, or, on a cylinder of diameter 100 μm, an increase in length of about 4 μm. Of course, much of this oxide was probably created near the interface with the substrate and a relatively small proportion ejected through the discharge channel onto the free surface. It's also possible that molten oxide gets

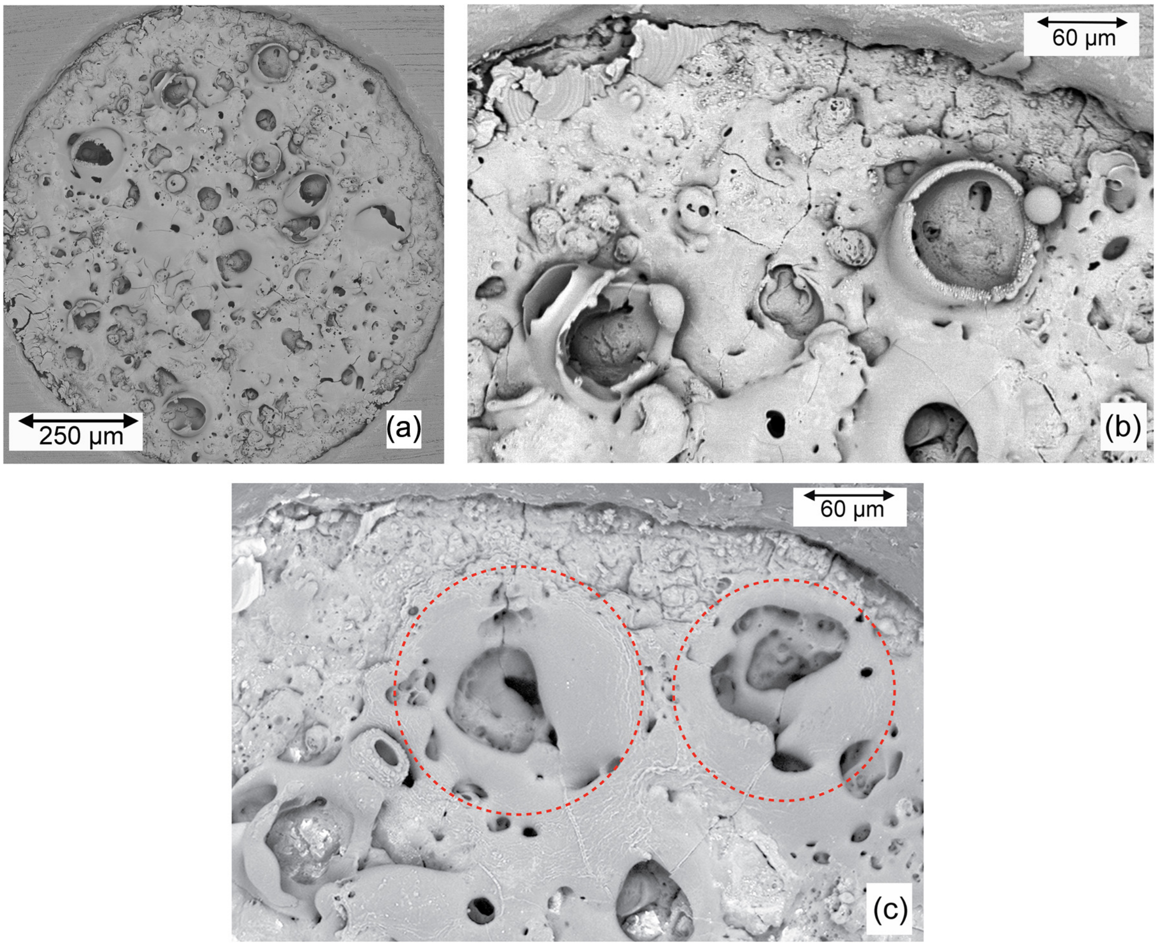

Fig. 3. SEM micrographs of a small area sample, with 100 μm PEO coating, showing (a) complete surface in initial state, (b) magnified top central region and (c) the same region after further PEO processing at 50 Hz for 1 s (with the regions in which the discharges were localised indicated by circles).

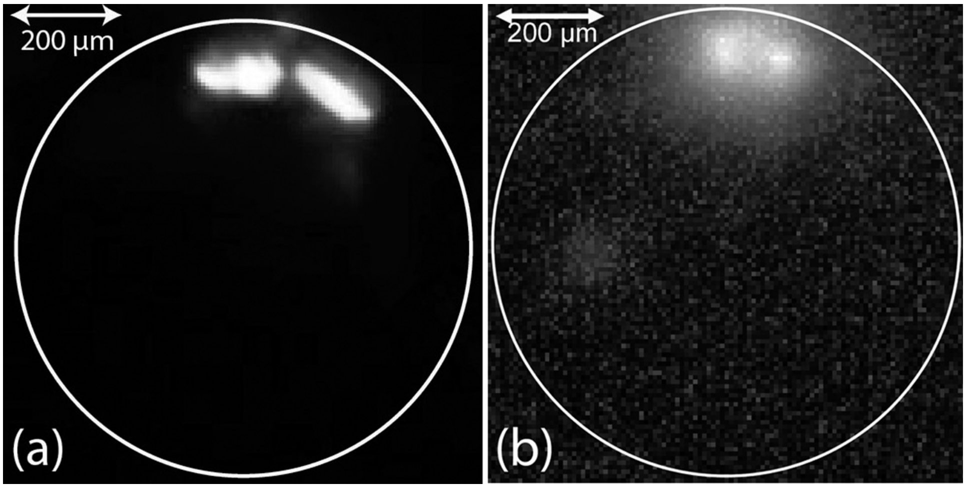

Fig. 4. Video images of the small area sample taken during the 1 s PEO treatment at 50 Hz (in the same orientation as Fig. 3), showing (a) a typical single frame and (b) the complete set of (~180,000) superimposed frames. The white circles show the approximate location of the sample boundary.

injected under the pressure of the discharge into neighbouring inter-connected pores – see §3.5 below. In any event, what is being observed in Fig. 3(b) and (c) appears to be at least broadly consistent with these expectations about the quantities of oxide involved.

3.3. Effect of a second interruption on discharge cascade localisation

The outcome of the experiment in which the sample was subjected to a second PEO treatment of duration 1 s (at 50 Hz), after

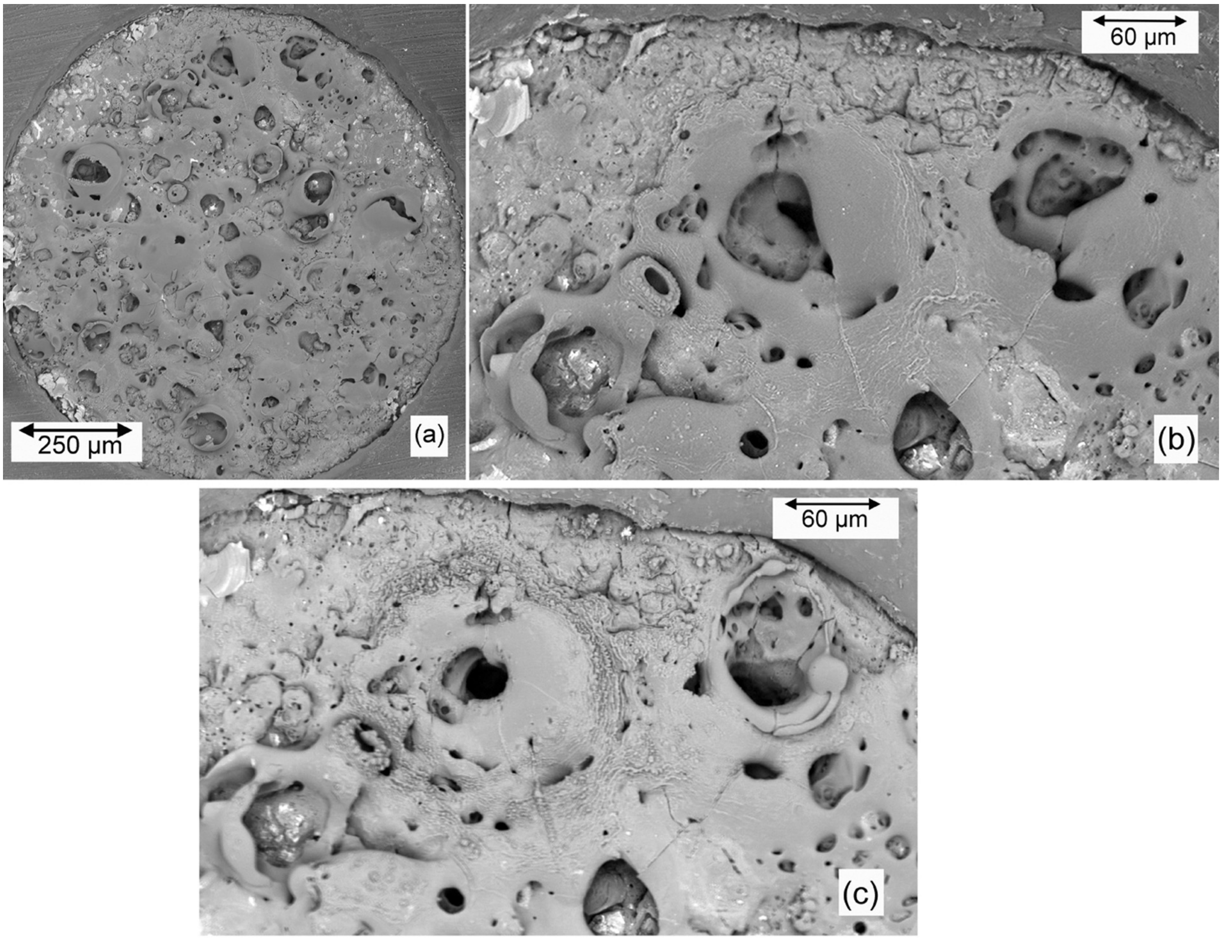

Fig. 5. SEM micrographs of a small area sample, with 100 µm PEO coating, showing (a) complete surface in the initial state (after one 1 s treatment), (b) magnified region where the cascade occurred and (c) the same region after PEO processing at 50 Hz for a further period of 1 s.

having been removed once and examined in the SEM, is presented in Fig. 5. This is an analogous set of micrographs to that in Fig. 3 and it can be seen that similar effects were observed, with a change in the surface appearance again having been created only in the upper central part of the section. (Fig. 5(b) is thus the same image as Fig. 3(c), which is reproduced here for ease of comparison with Fig. 5(c).) The associated video information was also similar to that shown in Fig. 4. It is clear from these observations that it is the residual microstructure (probably primarily the presence of pore channels) that predisposes a cascade of discharges to persist in the same location, rather than anything connected with residual thermal or electrical fields. It may also be noted that the total number of discharges in the cascade that extended through these two 1 s treatments was about 700. The maximum number of discharges in a cascade cannot really be estimated from the information here, although it seems likely that the figure might be of the order of at least 1000. Future work will involve protracted monitoring of discharge cascades, so as to cover their complete lifetimes, but it's already clear that the number of repeated discharges in the same location can be very large, and that the location must be favoured by a prominent feature that persists for extended periods (ie many discharges, and considerable conversion of substrate to oxide in the vicinity) and through the complete cessation of the processing. The most likely feature responsible for this behaviour is clearly a large, deep pore, or pore network, which, when (re)-filled with electrolyte, provides a path of low electrical resistance.

3.4. *Microstructural evolution with a high frequency supply*

The same operations were carried out (on a different sample), with a frequency of 2.5 kHz. The outcomes are shown in Fig. 6. In this case also, a discharge cascade occurred, localised in one place and extending over the treatment period of 1 s. The discharges were fairly uniformly distributed in time, with the total number during the period being about 150 (so that they occurred approximately once every 15 cycles, at intervals of about 6 ms). In this case, there was just one channel reaching the surface, and indeed it may well be relatively unusual for two nearby channels to be created as part of a single discharge cascade, as was observed in the 50 Hz case.

A significant difference, however, between outcomes with the low and high frequency supplies was the occurrence in the latter case of discharges during cathodic half-cycles, although they formed only sporadically. Fig. 7 shows a set of 6 images, each created by superimposing the 36 video frames that cover a half-cycle in the set for which the electrical data are shown in Fig. 2. Alternate images in this sequence thus cover anodic and cathodic half-cycles, starting with an anodic one. It can be seen that the half-cycles for which significant current flow took place (i.e. discharges occurred) correspond to ones in which there was light emission (i.e. all except the third one in this series). It's also clear that all of the discharges took place in the same location – the one shown in Fig. 6. Also apparent is that the cathodic discharges (second, fourth and sixth in this series) involved stronger light emission than the anodic

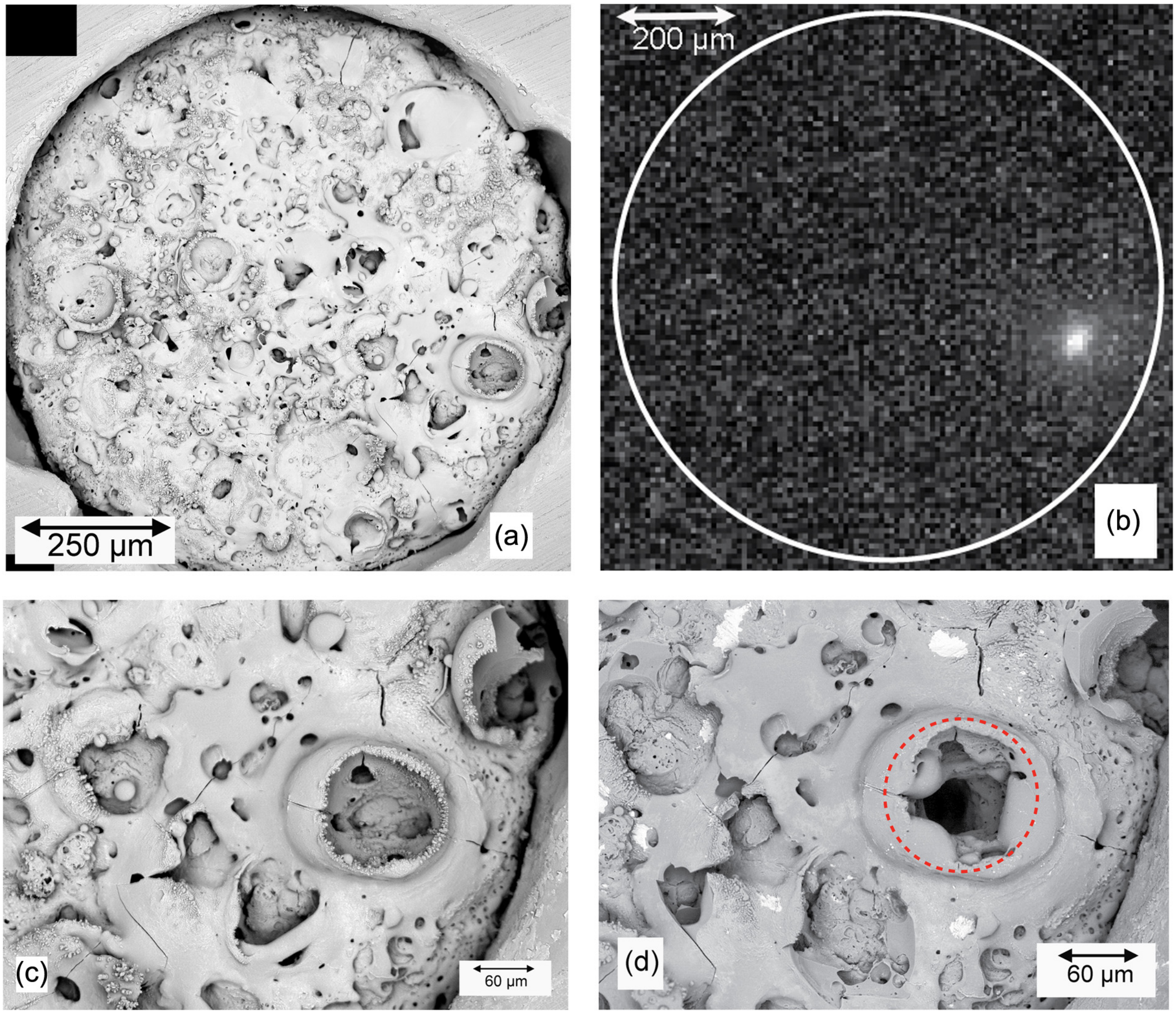

Fig. 6. Microstructural effects of a discharge cascade on a small area sample (with 100 μm PEO coating) at 2500 Hz for 1 s, showing (a) SEM micrograph of the surface in the initial state, (b) superimposed set of (~200,000) video images taken during the process, (c) magnified SEM of the region indicated in (b) as the cascade location and (d) the same area after PEO processing (with the region in which the discharges were localised indicated by circles).

ones. This is consistent with the associated currents (in Fig. 2) being significantly greater for the cathodic discharges.

Of course, since there were relatively few cathodic discharges during the experiments carried out here, and they occurred in the same locations as anodic ones in the cascade concerned, it's not really possible to draw any conclusions about the microstructural changes they induced. It seems likely, however, that they also promote at least some oxidation of the substrate (and possibly more than for the case of an anodic discharge, since they are more energetic).

3.5. *Tomographic study of discharge channel architecture*

An impression of the 3-D pore architecture of a discharge channel (immediately after a cascade in it has been completed) can be obtained from Fig. 8, which comprises a perspective view down into the channel, followed by a series of transverse sections. (The appearance is broadly consistent with recent work [22] showing tomographic data from PEO coatings.) It can be seen that, while the architecture is naturally rather irregular, the main pore does penetrate down close (a few microns) to the substrate, although it does taper slightly in diameter with increasing depth. It is a few tens of microns in diameter near the bottom, while the region of the "volcanic crater" at the top has a diameter of ~100 μm. The surrounding region at the top of the channel may be largely formed of oxide ejected from it during the cascade. It's possible that the "incubation period" between the individual discharges in a cascade (usually of the order of several hundred μs) represents the time needed for electrolyte to fill the (evacuated) channel left after the plasma in it has collapsed. This possibility will be explored in future work.

Of course, porosity in PEO coatings does tend to be interconnected. Furthermore, while they are certainly quite porous (typically [20] ~15–20%), they do not normally contain many very large diameter pores of the type seen here, at least in Al-based samples. The reason for this is presumably that they tend to become filled, or to collapse, when new discharges occur in the vicinity. It seems likely that molten oxide can be expelled from an active discharge channel, not only to the free surface (creating "volcanic craters"), but also into nearby residual pores from earlier cascades. In this way, the only large diameter through-thickness pores present in a PEO coating (of the type shown in Fig. 8) are likely to be those created by the most recent discharge cascades.

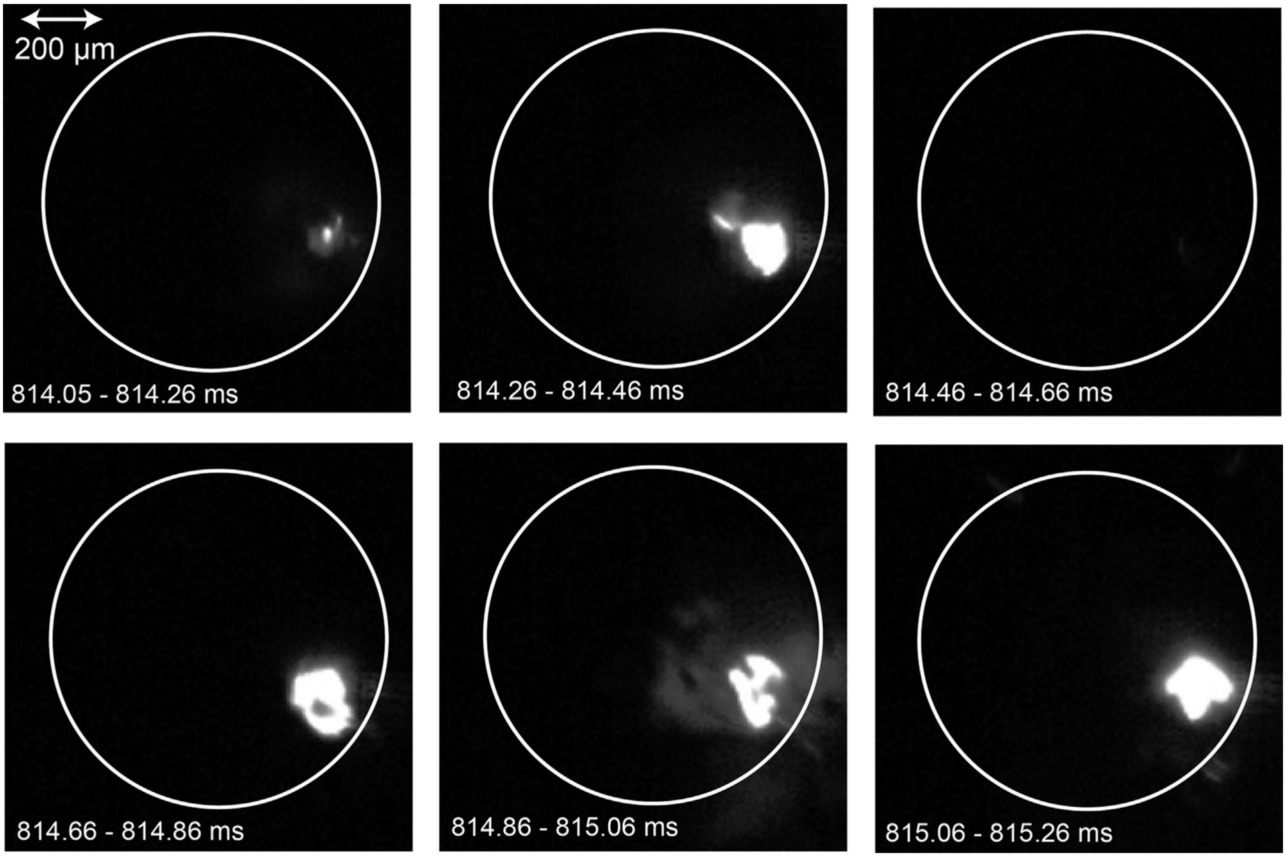

Fig. 7. Sequence of superimposed sets of video images (each made up of 36 separate images, covering one of the 6 half-cycle periods shown in Fig. 2), during PEO processing at 2.5 kHz.

4. Conclusions

The following conclusions can be drawn from the information presented here.

(a) It is confirmed that the discharges occurring during PEO have a strong tendency to take place in extended sequences (cascades) at fixed locations. These have been observed to comprise at least several hundred individual discharges and it seems likely that this number could commonly run into thousands.

(b) From microstructural observations of the changes induced by individual cascades on the free surface, the affected regions are approximately circular, with diameters of the order of 100 μm. From estimates of the aggregate discharge energy involved in a cascade of, say, 1000 discharges, and the relationship between this and the volume of oxide created, the associated increase in the average thickness of this circular area is ~5 μm. Eventually, this process presumably raises the electrical resistance of the region sufficiently for the cascade concerned to shut down.

(c) Tomographic reconstruction of the pore structure around a typical discharge channel (with a diameter of ~50 μm) revealed that it extended almost through the entire coating thickness (~100 μm in this case) to the substrate, where there was an oxide layer a few microns in thickness. The region of consumption of the substrate at the bottom of the pore channel extends down several microns, relative to the surrounding area.

(d) Discharges within a cascade continue at the same location, even if the PEO process is interrupted, the sample removed, dried and replaced in the electrolyte and the process restarted. This strongly suggests that it is residual microstructural features, particularly the pore channel, that are ensuring that the cascade persists in the same location, rather than short term effects such as residual thermal or electrical fields. The incubation period between discharges may represent the time required for these channels to become refilled with electrolyte.

(e) A high frequency supply, with the half-cycle period approaching typical discharge lifetimes, creates discharges at similar overall intervals to the low frequency case, also in spatially-localised cascades and inducing similar microstructural changes. It has also been observed that high frequency leads to discharges occurring during the cathodic half-cycle, as well as the anodic one. Furthermore, these cathodic discharges are more energetic than the anodic ones, although, within a cascade, they occur in the same locations as the anodic ones.

Acknowledgements

This work has been supported by EPSRC (grant number EP/I001174/1), by a Sims Scholarship (for SCT) in Cambridge University and by Keronite plc. Financial support (for AN) has also been received from the Fundacion Banco Santander, in the form of a Research Mobility Scholarship. The work is also related to the COST TD 1208 Network.

Thanks are due to Steve Hutchins and Suman Shrestha, of Keronite, for many helpful discussions, and the technical assistance of Kevin Roberts (Cambridge) is also gratefully acknowledged. In compliance with EPSRC requirements, raw data in the form of selected video and discharge current files, and also the tomographic reconstruction data, are available at www.ccg.msm.cam.ac.uk/publications/resources, and are also accessible via the University repository at http://www.data.cam.ac.uk/repository.

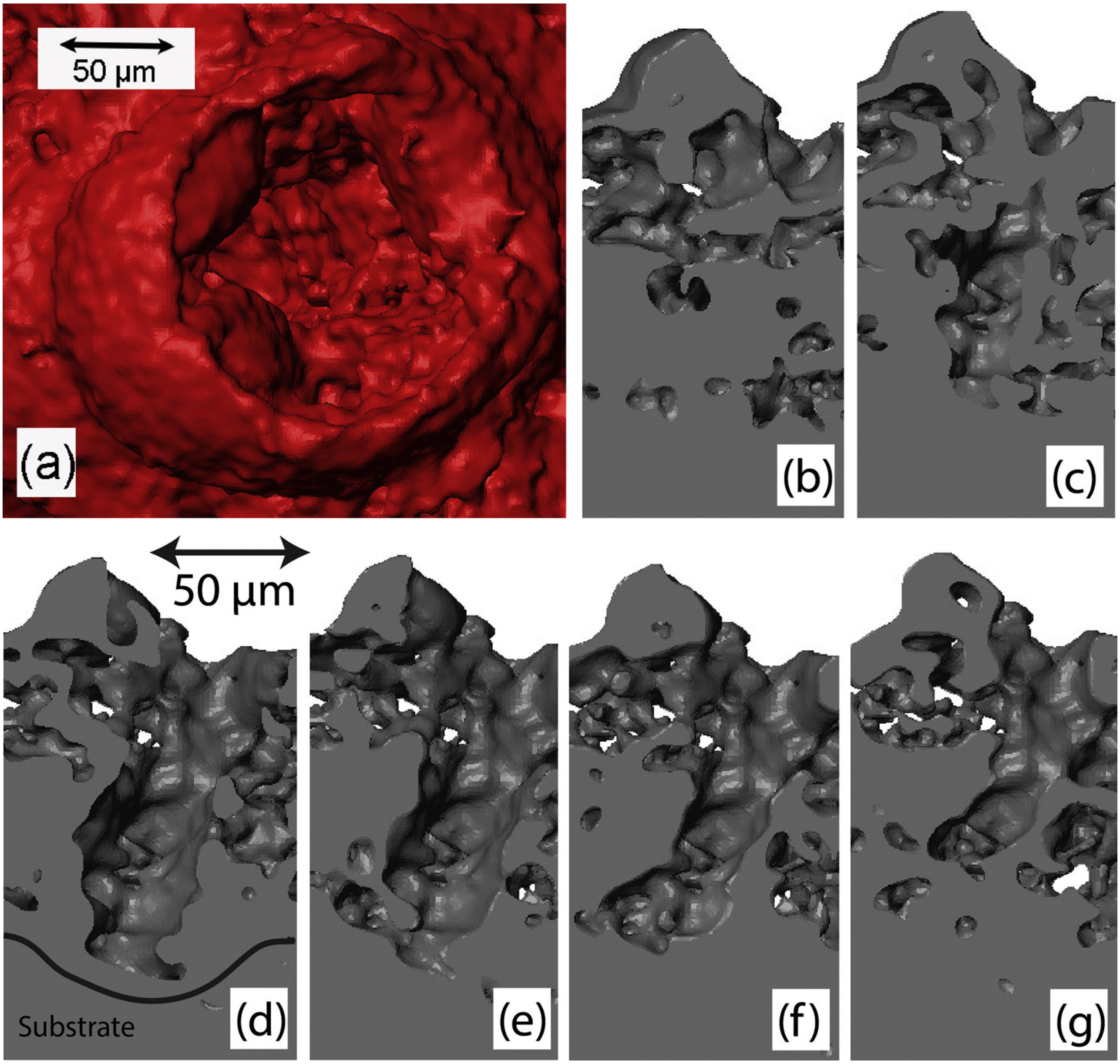

Fig. 8. Tomographic data from the region of the small area sample in Fig. 6(d), showing (a) a perspective view into the pore channel and (b)–(g) progressive parallel sections (11 µm apart), containing the through-thickness direction, with sections (d) and (e) located near to the approximate axis of the pore.

References

[1] C.S. Dunleavy, I.O. Golosnoy, J.A. Curran, T.W. Clyne, Characterisation of discharge events during plasma electrolytic oxidation, Surf. Coat. Technol. 203 (22) (2009) 3410–3419.

[2] C.S. Dunleavy, J.A. Curran, T.W. Clyne, Self-similar scaling of discharge events through peo coatings on aluminium, Surf. Coat. Technol. 206 (6) (2011) 1051–1061.

[3] R.O. Hussein, D.O. X Nie, A. Northwood, Spectroscopic and microstructural study of oxide coatings produced on a Ti–6Al–4 V alloy by plasma electrolytic oxidation, Mater. Chem. Phys. 134 (1) (2012) 484–492.

[4] C.S. Dunleavy, J.A. Curran, T.W. Clyne, Time dependent statistics of plasma discharge parameters during bulk AC plasma electrolytic oxidation of aluminium, Appl. Surf. Sci. 268 (0) (2013) 397–409.

[5] J. Martin, A. Melhem, I. Shchedrina, T. Duchanoy, A. Nomine, G. Henrion, T. Czerwiec, T. Belmonte, Effects of electrical parameters on plasma electrolytic oxidation of aluminium, Surf. Coat. Technol. 221 (2013) 70–76.

[6] A. Nomine, S.C. Troughton, A.V. Nomine, G. Henrion, T.W. Clyne, High speed video evidence for localised discharge cascades during plasma electrolytic oxidation, Surf. Coat. Technol. 269 (2015) 125–130.

[7] S.C. Troughton, A. Nomine, A.V. Nomine, G. Henrion, T.W. Clyne, Synchronised electrical monitoring and high speed video of bubble growth associated with individual discharges during plasma electrolytic oxidation, Appl. Surf. Sci. 359 (2015) 405–411.

[8] A. Melhem, G. Henrion, T. Czerwiec, J.L. Briancon, T. Duchanoy, F. Brochard, T. Belmonte, Changes induced by process parameters in oxide layers grown by the PEO process on Al alloys, Surf. Coat. Technol. 205 (2011) pS133–S136.

[9] H. Habazaki, S. Tsunekawa, E. Tsuji, T. Nakayama, Formation and characterization of wear-resistant peo coatings formed on β-titanium alloy at different electrolyte temperatures, Appl. Surf. Sci. 259 (2012) 711–718.

[10] E. Matykina, R. Arrabal, A. Pardo, M. Mohedano, B. Mingo, I. Rodriguez, J. Gonzalez, Energy-efficient PEO process of aluminium alloys, Mater. Lett. 127 (2014) 13–16.

[11] L. Wang, W. Fu, L. Chen, Evolution of active species and discharge sparks in na2sio3 electrolyte during PEO process, J. Alloys Compd. 509 (28) (2011) 7652–7656.

[12] A. Hamdan, C. Noel, F. Kosior, G. Henrion, T. Belmonte, Dynamics of bubbles created by plasma in heptane for micro-gap conditions, J. Acoust. Soc. Am. 134 (2) (2013) 991–1000.

[13] S.P. Sah, E. Tsuji, Y. Aoki, H. Habazaki, Cathodic pulse Breakdown of anodic films on aluminium in alkaline silicate electrolyte – understanding the role of cathodic half-cycle in AC plasma electrolytic oxidation, Corros. Sci. 55 (2012) 90–96.

[14] A. Nomine, J. Martin, C. Noel, G. Henrion, T. Belmonte, I.V. Bardin, V.L. Kovalev, A.G. Rakoch, The evidence of cathodic micro-discharges during plasma electrolytic oxidation process, Appl. Phys. Lett. 104 (8) (2014) (p.Art. 081603).
[15] A. Nomine, J. Martin, G. Henrion, T. Belmonte, Effect of cathodic micro-discharges on oxide growth during plasma electrolytic oxidation (PEO), Surf. Coat. Technol. 269 (2015) 131–137.
[16] A.G. Rakoch, A.A. Gladkova, Z. Linn, D.M. Strekalina, The evidence of cathodic micro-discharges during plasma electrolytic oxidation of light metallic alloys and micro-discharge intensity depending on ph of the electrolyte, Surf. Coat. Technol. 269 (2015) 138–144.
[17] R.O. Hussein, X. Nie, D.O. Northwood, An investigation of ceramic coating growth mechanisms in plasma electrolytic oxidation (PEO) processing, Electrochim. Acta 112 (2013) 111–119.
[18] X.P. Lu, C. Blawert, Y.D. Huang, H. Ovri, M.L. Zheludkevich, K.U. Kainer, Plasma electrolytic oxidation coatings on Mg alloy with addition of SiO_2 particles, Electrochim. Acta 187 (2016) 20–33.
[19] X.P. Lu, C. Blawert, K.U. Kainer, M.L. Zheludkevich, Investigation of the formation mechanisms of plasma electrolytic oxidation coatings on Mg alloy am50 using particles, Electrochim. Acta 196 (2016) 680–691.
[20] J.A. Curran, T.W. Clyne, Porosity in plasma electrolytic oxide coatings, Acta Mater. 54 (7) (2006) 1985–1993.
[21] X.W. Yu, L. Chen, H.L. Qin, M.Y. Wu, Z.C. Yan, Formation process of in situ oxide coatings with high porosity using one-Step plasma electrolytic oxidation, Appl. Surf. Sci. 366 (2016) 432–438.
[22] X. Zhang, S. Aliasghari, A. Nemcova, T.L. Burnett, I. Kubena, M. Smid, G.E. Thompson, P. Skeldon, P.J. Withers, X-ray computed tomographic investigation of the porosity and morphology of plasma electrolytic oxidation coatings, ACS Appl. Mater. Interfaces 8 (13) (2016) 8801–8810.
[23] J. Dean, T. Gu, T.W. Clyne, Evaluation of residual stress levels in plasma electrolytic oxidation coatings using a curvature method, Surf. Coat. Technol. 269 (2015) 47–53.